



Multi-station electro-optical observations of the 1999 Leonid meteor storm

P. Brown^{a,b,*}, M.D. Campbell^a, R.L. Hawkes^c, C. Theijsmeijer^a, J. Jones^a

^aDepartment of Physics and Astronomy, University of Western Ontario, London, Ontario, Canada N6A 3K7

^bLos Alamos National Laboratory, EES-D, MS J577, Los Alamos, NM 87545, USA

^cPhysics Department, Mount Allison University, 67 York Street, Sackville, N.B., Canada E4L 1E6

Received 20 March 2001; accepted 23 July 2001

Abstract

Single- and double-station video observations of the 1999 Leonid shower made from Israel are presented. A total of 232 double-station Leonids had trajectories computed. Additionally, some 2500 single-station Leonids were used to measure the Leonid storm flux and mass distribution in the interval from 0.5–3 UT 18 November 1999. The height distribution for storm Leonids of average mass $\sim 10^{-6}$ – 10^{-7} kg indicates that the ablation zone is approximately Gaussian-shaped with best-fit mean begin, maximum brightness and end heights of 123.3 ± 0.7 , 107.3 ± 0.42 and 95.0 ± 0.56 km respectively. The peak flux at the time of the storm was found to be 0.81 ± 0.06 meteoroids $\text{km}^{-2} \text{hr}^{-1} \text{Mv} < +6.5$ using 15 min binning and 0.99 ± 0.11 meteoroids $\text{km}^{-2} \text{hr}^{-1} \text{Mv} < +6.5$ for 3 min intervals. The smaller temporal resolution reveals a broad plateau in flux lasting from approximately $\lambda_0 = 235.276$ – 235.285° (J2000.0). At least one significant feature in the rate curve is apparent near 235.272° , which we suggest is associated with material released in 1932. The video mass distribution index over the course of the Leonid storm was found to be constant near $s = 1.75$. The peak time of the storm estimated from 15 min sampling of the flux profile is near $235.283 \pm 0.005^\circ$ (1h58m \pm 7m) while 3 min resolution data place the maximum at $235.281 \pm 0.003^\circ$ (1h55m \pm 4m). The mean radiant position at the time of the storm was found to be $\alpha = 153.1 \pm 0.1^\circ$ and $\delta = 21.5 \pm 0.2^\circ$ (J2000), with some hint of a more compact radiant grouping within the range $\alpha = 153$ – 154° and $\delta = 21$ – 22° . We do not find evidence for any significant high altitude Leonid population at video masses despite biasing one camera pair to an intersection altitude of 160 km. © 2002 Elsevier Science Ltd. All rights reserved.

Keywords: Meteors; Meteor shower; Leonids; Meteor storm; Electro-optical observations

1. Introduction

The 1999 return of the Leonid meteor shower was widely predicted to reach storm proportions on 18 November near 2 UT (cf. Yeomans et al., 1996; McNaught and Asher, 1999b; Brown, 1999). Indeed, a significant Leonid storm transpired on that night, visible primarily at mid-Eastern longitudes (Arlt et al., 1999). The characteristics of meteoroids associated with the storm component of the Leonids in 1999 is of particular interest as these meteoroids are very young (2–3 revolutions old, cf. McNaught and Asher, 1999b) and therefore might be expected to show physical differences as compared to older Leonids. Physical properties of older Leonids have been studied during the 1998 Leonid shower using several methods (Campbell

et al., 2000; Simek and Pecina, 2001; Brown and Arlt, 2000; Spurny et al., 2000). In particular, the heights of ablation, trail lengths and relationship between mass, magnitude and entry angle for “storm” Leonids in 1999 may provide indirect statistical evidence for any relative physical differences between the storm and older components of the stream seen in 1998. The apparent success of the dustball model for the 1997 and 1998 Leonid return (cf. Campbell et al., 1998; Murray et al., 1999; Campbell et al., 2000; Murray et al., 2000) also places specific constraints on the expected behaviour of the begin and end heights of Leonids as a function of mass. Additionally, details of the flux and mass distribution within the 1999 storm provide additional constraints for the formation and evolution of the stream which any successful model needs to reproduce.

Here we present results for the mass distribution, flux, and height distribution of the 1999 Leonids, based on multi-station electro-optical observations made in Israel. Preliminary results from the global ground-based Leonid

* Corresponding author. Tel.: +1-505-665-7134; fax: +1-505-667-9122.

E-mail address: pbrown@lanl.gov (P. Brown).

campaign (of which these data are a part) in 1999 have been presented in Brown et al. (2000). Procedures used for single and double station analysis, positional analysis and photometric measurements have been covered in detail elsewhere (Campbell et al., 2000; Brown et al., 2000) and will not be repeated here. In total, some 1097 Leonids have been identified on tape, digitized, measured and fully reduced (including positional, photometric and double station analysis for some) out of a total sample of 3619 meteors which have been identified on the tapes but not fully analysed. Just over approximately 2500 of this total are Leonids. All these data were gathered on the main peak night (18 November 1999) of the Leonid storm from stations in Israel.

2. Equipment and observing sites

The 1999 ground-based Leonid campaign had coverage from seven different geographical sites (cf. Brown et al. (2000) for details). Here we concentrate on data gathered by five cameras deployed at two sites in Israel on the night of 18 November 1999 from 0h30m–3h30m UT, centered about the nominal observed peak just after 2 UT (Arlt et al., 1999).

Two stations were set up, one at the Wise Observatory, near Mitzpe Ramon, Israel (30° 35' 45" N, 34° 45' 48" E) and the other near Revivim Kibbutz, Israel (31° 1' 45" N, 34° 42' 30" E). These were used in a triangulation mode (baseline 48.5 km) with four microchannel plate (MCP) image intensified CCD cameras at each location. Two image intensifiers at each site were generation II devices and two were generation III. The total spectral response extends from about 340–870 nm, although the generation III response is stronger in the red and near infrared than for the generation II systems which employ a near visual S-20 photocathode. Different focal length lenses were used at each site, resulting in different fields of view and limiting sensitivities, in order to extend the mass regime for determination of the mass distribution index. C-mount objective lenses with focal lengths from 25 to 75 mm were used, producing fields of view ranging from 35° to 9°, and a maximum limiting stellar magnitude on the most sensitive systems of nearly +9^M. The limiting meteoroid mass for the most sensitive cameras was approximately 2×10^{-8} kg for Leonid meteors. One of the systems at the Wise Observatory used a 200 lines per mm blazed grating for low resolution spectra and recorded almost 100 Leonid spectra during the course of the storm, but has not been fully analysed as yet and will not be discussed further here. All CCD cameras used in the campaign were Cohu model 4910 scientific monochrome units operated at NTSC video frame rates (30 fps, with two interlaced video fields per frame). The Gen II systems were Litton MILSPEC intensifiers and used macro-lens to couple the CCD to the back of the image intensifiers. The Gen III systems were NiteMate model micro-channel plated, fibre-optically coupled inten-

Table 1

Summary of Israel camera statistics analysed to date for data gathered during the Leonid peak (UT 18 November 1999)^a

Camera letter/time (UT)	Number of meteors	Number of Leonids
E 2030–2230	2230–0030	82
	0030–0230	381
	0230–0315	68
		19
F 2030–2230	2230–0030	59
	0030–0230	512
	0230–0315	66
		24
G 2030–2230	2230–0030	32
	0030–0230	135
	0230–0315	30
		16
J 2030–2230	2230–0030	92
	0030–0230	274
	0230–0315	52
		21
K 2030–2230	2230–0030	
	0030–0230	285
	0230–0315	55
		221
T 2030–2230	2230–0030	111
	0030–0230	790
	0230–0315	128
		37

^aCamera O recorded no useable data due to a VCR fault.

sifier tubes manufactured by Litton. The video output from each camera was recorded directly to VHS tape and later digitized directly from the same tape.

Data were recorded on the nights of 15, 16, 17 and 18 November from 2230–0530 local time each night. For the two Israeli sites, the cameras were pointed to common volumes in the atmosphere to permit double-station measurements with the video systems (see Campbell et al., 2000 for details of the procedure). Only data for the peak night (18 November 2000) will be described here.

The number of meteors recorded from each of the Israeli stations are given in Table 1. Unfortunately, camera O had a recording problem and no useable data was gathered from it for the night of the peak (17/18 November 1999). The cameras were left in fixed geometry mode throughout the night.

The sensitivity for each of the cameras is shown in Table 2. The effective meteor limiting magnitude measures the equivalent limiting magnitude to which all Leonids would be detected given the actual numbers recorded. Fig. 1 demonstrates the method used to obtain this value for a typical camera.

Table 2

Limiting effective stellar magnitude sensitivities of the four cameras for which detailed analyses have been performed on 18 November 1999^a

Camera designation	Limiting magnitude	Collecting area (km ²)
E (Gen II–25 mm lens–FOV 28° × 21°)	+2.1 (+7.6)	6380
F (Gen II–25 mm lens–FOV 35° × 26°)	+2.1 (+7.8)	7643
J (Gen III–50 mm lens–FOV 20° × 15°)	+2.6 (+8.6)	3052
T (Gen III–25 mm lens–FOV 21° × 28°)	+3.3 (+8.4)	10433
K (Gen III–50 mm lens–FOV 11° × 14°)	+3.8 (+8.7)	1907

^aThe first value is the effective limiting magnitude of the camera for Leonids (i.e. the camera sees all Leonids brighter than this value with no losses), while the second number in brackets is the limiting stellar magnitude for the camera. Note that the spectral responses are different for Gen II and Gen III systems, with the latter being more sensitive at longer wavelengths. FOV=Field of view (horizontal × vertical). The physical collecting area for each camera field at the time of the Leonid peak on the night of 18 November 1999 is given in the third column. This physical collecting area does not take into account the change in radiant elevation.

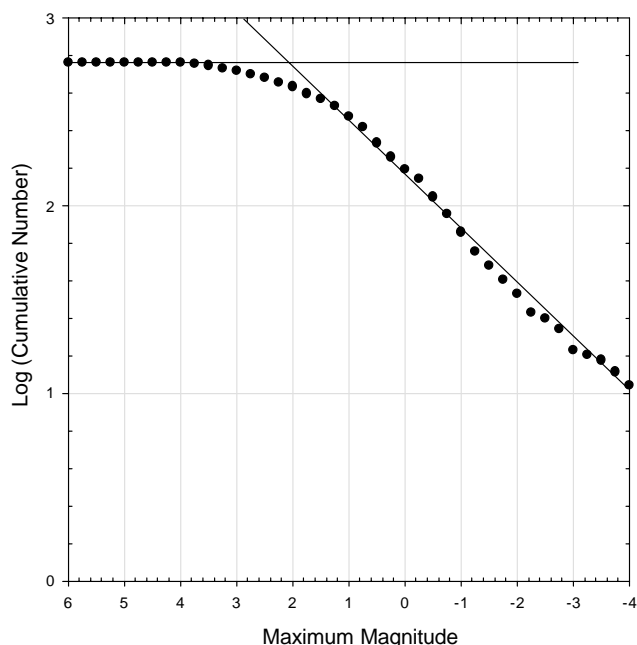


Fig. 1. The cumulative number of Leonids versus the maximum measured magnitude on the night of 18 November 1999 for camera E. The meeting point for the two asymptotes shown represents the “effective” limiting magnitude for which the camera equivalently detects all Leonids. The total number of Leonids in this sample is 579.

3. Results

3.1. Mass distribution

The mass distribution index is a measure of how rich a shower is in faint meteors. Most showers follow the relation

$$N_C = \frac{C}{1-s} m^{1-s}, \quad (1)$$

where N_C is the cumulative number of meteors with masses greater than m , C is a constant and s is the mass distribution index.

Taking the logarithm of both sides will give a linear relation between $\log N_C$ and $\log m$, with a slope of $1-s$. A high s value indicates that a shower is rich in faint meteors:

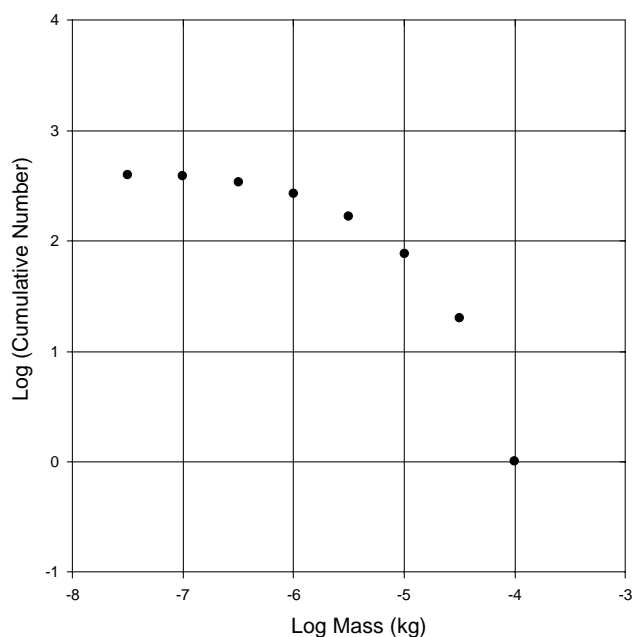


Fig. 2. Typical Leonid mass distribution (camera E).

that is, there are many more faint meteors than bright ones. A low s value indicates that the number of meteors does not greatly increase at higher magnitudes.

Note that our measured mass values are the sum of the integrated light measured frame by frame for each meteor (see Hawkes (2002) for more details). As a result, we expect the relative differences in mass to be more accurate than simply using the maximum magnitude as a measure of the total mass. In converting from magnitude to photometric mass, it is assumed that the luminous efficiency factor depends linearly on velocity and we used the value of the luminous efficiency factor as determined by Verniani (1965).

We plot above the log cumulative number versus log mass for the Leonid meteors from 1999 with photometric masses for a typical camera for which photometry was performed (Fig. 2). Note that photometric reduction of camera T was not possible due to the large number of Leonids involved and poor photometric calibration of the video images. We

also note that the photometric estimates for brighter Leonids are inferred from stellar photometric relations derived from fainter stellar sources (generally +1 and fainter) and extrapolated to the brighter magnitudes. As a result, Leonid magnitudes brighter than approximately -2 are quite uncertain. The magnitudes used are apparent, but the high elevation of the camera pointing directions implies that the ranges are not significantly different from 100 km and hence the correction to absolute magnitude would be small in most cases. The magnitudes are derived from comparison stars in the V system. As a result the magnitudes for the Gen II systems are approximately V, while those for the Gen III systems have more sensitivity into the IR.

When the faintest data are excluded (because of incomplete recovery of faint meteors — a typical adopted slope used to find s is shown in Fig. 1) the mass distribution index is measured to be $s = 1.75$ for all but camera J (where $s = 1.54 \pm 0.05$ was measured). One bias in this measurement is the fact that some meteors either begin or end outside the field of view, a particular problem for narrow camera fields (like cameras J and K). To determine if this bias introduced a significant systematic offset in the mass distribution numbers, the same mass distribution data were used again, but only meteors beginning and ending on the screen were kept. The resulting values for the mass index for all Leonids are compared with the total Leonid sample in Fig. 3. There is no clear systematic shift apparent for all cameras — indeed much of the observed change may simply be due to the smaller number statistics in the on-screen sub-sample. These measurements at the time of the peak are in general agreement with $s = 1.64 \pm 0.06$ value derived for the 20 min period around the storm peak using video instruments by Gural and Jenniskens (2000) and the $s = 1.8 \pm 0.2$ found by Rendtel et al. (2000) from video data and $s \sim 1.9 \pm 0.1$ found by Arlt et al. (1999) from visual data.

The mass distribution samples were broken down into time intervals for which at least 50 or more Leonids were available for a single measurement of the mass distribution index. This was in an attempt to determine if any significant changes in the mass distribution occurred across the Leonid stream cross-section. In general, even with 50–80 Leonids in each measurement of the mass index, no consistent systematic change in the mass distribution index across the stream is visible for all cameras. Hence, we were unable to find any statistically significant changes in the mass distribution index between $\lambda_0 = 235.23\text{--}235.32^\circ$ over intervals longer than 20 min, either due to intrinsic lack of variation within the stream or small number statistics.

There is a weak hint in camera E data that a steeper drop-off may also be occurring at larger masses through this trend is not clear in any other camera. This large end roll-off was noted by Arlt et al. (1999) in visual data. A roll-off at fainter magnitudes reported by Arlt et al. (1999) and Rendtel et al. (2000) is not evident in these distributions. It is possible that this trend in the visual data may be more an effect of the changing perception probabilities under storm condi-

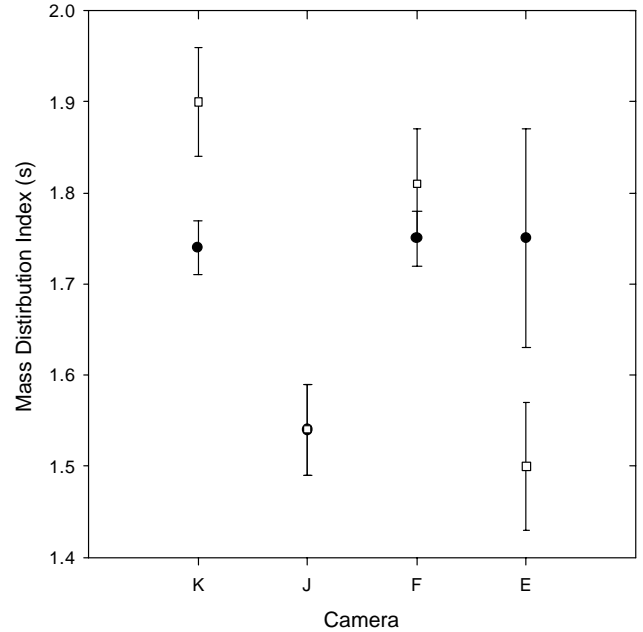


Fig. 3. Mass index measured for all Leonids (filled circles) and for only those Leonids which begin and end on screen (open squares).

tions rather than a genuine effect. The effect in Rendtel et al. (2000) could be due to even smaller number statistics than are used here. Comparison with the small sporadic sample measured during the same interval showed no clear differences between the shapes of the shower versus non-shower sample.

3.2. Video Leonid storm flux

The raw shower rates recorded by all cameras are shown in Figs. 4 and 5 with 15 and 3 min resolution, respectively. Note that all times have been topocentrically corrected according to McNaught and Asher (1999a), amounting to a 1 min correction.

The overall shape of the broad profile is well defined with the large 15 min binning — it shows a slightly asymmetric profile with a longer ascending than descending branch. The short-time resolution profile shows numerous small-scale features. Note that these are simply combined raw observed rates corrected for elevation of the radiant only.

To convert to a true flux of Leonids at the top of the atmosphere, we must first compute the physical collecting area of each camera projected onto the meteor zone in the atmosphere. Fig. 6 shows the basic geometry for a given camera field. Taking the (angular) vertical field of view to be v_f , the horizontal field of view to be h_f and the height (H) of the centre of the meteor zone (typically 100 km), the range from the camera to the top of the projection of the camera field onto the meteor zone is given by

$$R_{vt} = H / \sin\left(e + \frac{v_f}{2}\right), \quad (2)$$

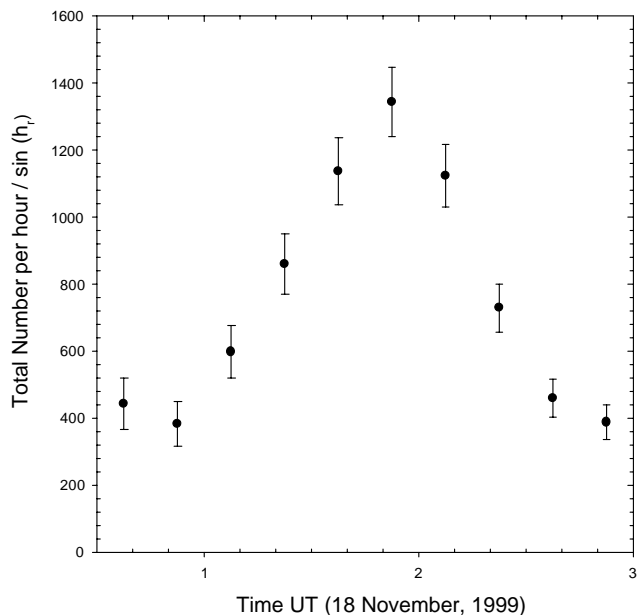


Fig. 4. Combined hourly rates of Leonids from all cameras binned into 15 min intervals and corrected for radiant altitude. All Leonids appearing in the field of view have been counted.

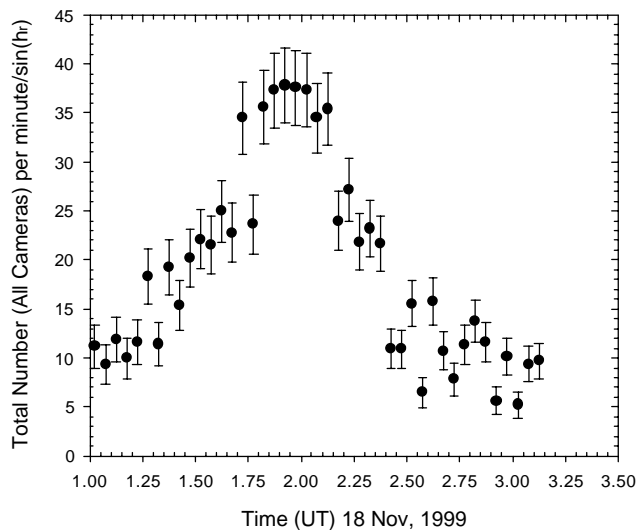


Fig. 5. Combined minute rates of Leonids from all cameras binned into 3 min intervals and corrected for radiant altitude.

where e is the elevation of the centre of the camera field of view in degrees. Similarly, the range to the bottom of the field of view can be found as

$$R_{vb} = H / \sin\left(e - \frac{v_f}{2}\right). \quad (3)$$

The linear distance of the projection along the sides of the camera field at the height of the meteor zone is then given by

$$V_1 = \sqrt{R_{vt}^2 + R_{vb}^2 - 2R_{vt}R_{vb} \cos(v_f)}. \quad (4)$$

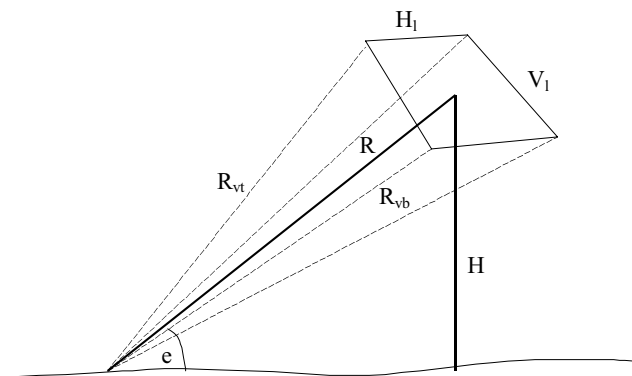


Fig. 6. Geometry for calculation of the physical collecting area for a video system. R_{vt} is the range from camera to the top of the video field, R_{vb} is the range at the bottom of the video field, and R is the range to the middle of the video field at height H . H_1 is the horizontal distance across the top of the trapezoidal-shaped video field and V_1 is the vertical distance across the sides of the trapezoid.

The range, R , to the centre of the field of view can be found simply from

$$R = H / \sin e. \quad (5)$$

Similarly, the horizontal linear distance of the camera field projected onto the meteor zone will be

$$H_1 = 2R \tan\left(\frac{h_f}{2}\right). \quad (6)$$

The final physical collecting area is then given as

$$\Theta = H_1 V_1. \quad (7)$$

We note that this simple calculation has been done ignoring the effects of the Earth's curvature. We have also assumed that the meteors are confined to a limited distribution of ranges. For most cases where $e > 30^\circ$, these approximations work very well and Eq. (7) produces a good estimate for the physical collecting area of the system accurate to better than 5%.

The physical collecting areas for each camera calculated in this way are given in Table 2. Note that edge effects due to decreased sensitivity for some of the Gen II systems are not taken into account here — for those systems in particular, these values are somewhat overestimated (by less than $\sim 10\%$). We use a constant $s = 1.75$ for all computations. Taking the radiant-altitude corrected rates (i.e. dividing the rates by $1/\cos(z)$ where z is the zenith angle of the radiant) given in Figs. 4 and 5 together with the physical collecting area for each camera, we may calculate the flux directly by dividing the rate by the collecting area. The resulting values for each camera are referenced to an equivalent limiting magnitude of +6.5 for ease of comparison with visual data, using the derived mass distribution index for each camera and its limiting magnitude. The final fluxes for each camera show some scatter due to small number statistics (for the smaller 3 min time intervals) and some effects due to

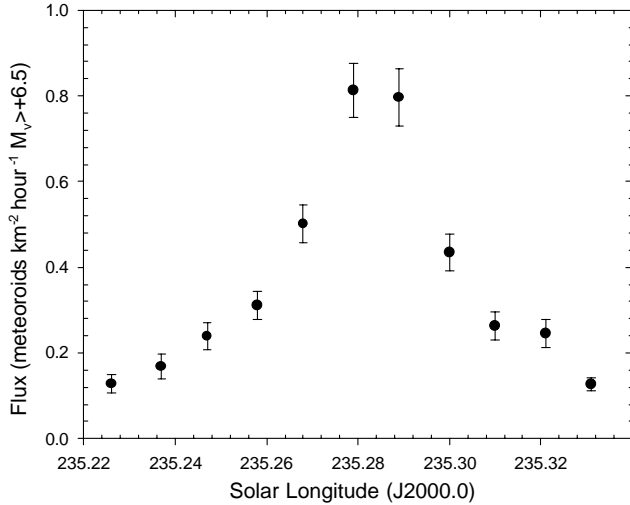


Fig. 7. The mean flux profile found from all five useable cameras on 18 November 1999 centred about the peak of the Leonid storm averaged in 15 min intervals as a function of solar longitude. Each point is the weighted mean of five measurements, each measured flux being weighted by its formal error margin.

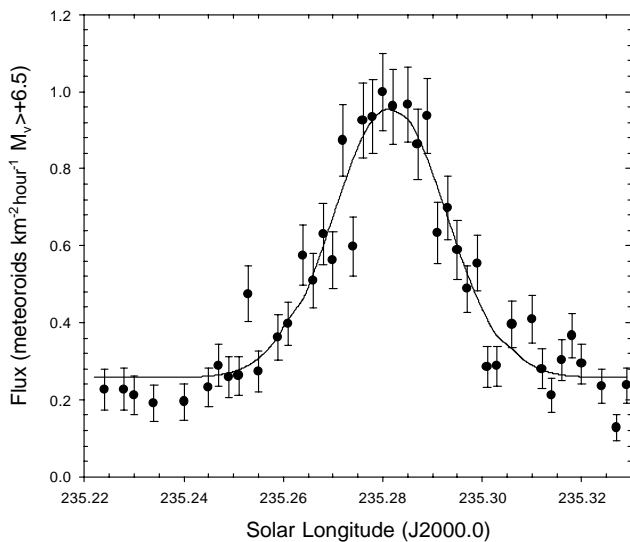


Fig. 8. The mean flux profile found from all five useable cameras on 18 November 1999 centred about the peak of the Leonid storm averaged in 3 min intervals as a function of UT time. Each point is the weighted mean of five measurements, each measurement being weighted by its formal error margin. The solid curve is a modified-Gaussian fit (see text for details).

errors in the measured limiting magnitudes for each camera as well as non-uniformity in detection across the video fields. Assuming these errors are largely random, we choose to take the absolute fluxes at 3 and 15 min intervals and compute a mean flux for all five cameras, weighting the averages using the formal error margins for each datum. This result is shown in Figs. 7 and 8. No correction for longer

trail lengths earlier in the evening have been made, though we estimate this effect to be smaller than the statistical error margins earlier in the night.

Our resulting mean profile using 15 min counts of all Leonids (including partial trails) shows a peak flux of 0.81 ± 0.06 meteoroids $\text{km}^{-2} \text{hr}^{-1} M_v < +6.5$. This flux value is in good agreement with the 0.82 ± 0.19 meteoroids $\text{km}^{-2} \text{hr}^{-1} M_v < +6.5$ derived by Gural and Jenniskens (2000) based on video data. Using the median $s = 1.75$, this corresponds to an equivalent visual ZHR of 4000 ± 300 binned over these 15 min intervals. This compares well with the visually determined ZHR value of 4100 found by Jenniskens et al. (2000) from visual and video data (1 and 2.8 min binning, respectively) and from Arlt et al. (1999) who found a peak ZHR of 3700 ± 100 for 2.8 min binned visual data. The full-width to half-maximum (FWHM) for this broad profile is found to be 54 min, in excellent agreement with the range of FWHM from 47 to 52 min found by Rendtel et al. (2000) based on video data. The ascending branch is found to be 29 min and the descending 25 min, showing the same pre-maximum asymmetry reported by Rendtel et al. (2000).

As expected, the shorter time profile shows both a higher peak flux and larger error margins per datum. The maximum flux was found to be 0.99 ± 0.11 meteoroids $\text{km}^{-2} \text{hr}^{-1} M_v < +6.5$ for 3 min binning, which is an equivalent ZHR of 4900 ± 600 .

The peak time estimated from the larger temporal sampling of the flux profile is near $235.283 \pm 0.005^\circ$ (1h58m \pm 7m), in good agreement with the peak times derived visually by Arlt et al. (1999) of $235.286 \pm 0.001^\circ$, by Singer et al. (2000) of $235.288 \pm 0.002^\circ$ found from combined radar and video data through wavelet analyses and $235.285 \pm 0.001^\circ$ by Jenniskens et al. (2000) from hybrid visual-video observations. These also are in general agreement with the formal peak from the higher temporal resolution data of $235.281 \pm 0.003^\circ$.

Two noticeable short-term fluctuations (greater than 2σ from surrounding datapoints relative to the general trend) are visible in the high-time resolution data — one at 01:16 UT (235.253°) and another near 01:42–01:46 UT ($235.272 - 235.274^\circ$). In both cases, all cameras showed enhanced activity in the relevant 3 min time bin. The latter enhancement is the most significant and is coincident with a similar enhancement visible in visual data collected from the middle-East, which showed an enhancement from 01:40 to 01:43 UT (Arlt et al., 1999). Rendtel et al. (2000) also report an activity “plateau” lasting from 01:39 to 01:53 UT in video data collected from Jordan. The timing of this feature is very close to that expected for material released from 55P/Tempel-Tuttle during its 1932 passage (maximum expected at 01:44 UT) (McNaught and Asher, 1999b). Whether these are of a physical origin (representing some material input from 1932 for example) or just statistical fluctuations in the stream is not clear.

The overall shape of the profile in the interval from 0.5 to 3 UT can be well-fit using a modified Gaussian of the form:

$$\Phi = \Phi_0 + a \exp \left[-0.5 \left(\frac{(t - t_0)}{w} \right)^2 \right], \quad (8)$$

where Φ is the flux, w is the Gaussian half-width of the distribution, Φ_0 is the background flux in this interval and t is the time in UT. This fit only works well within 1–2 h of the main peak, inclusion of further activity away from this time is better fit with a Lorentzian (cf. Jenniskens et al., 2000).

For the 3 min flux profile, the fit “centre” or maximum time was found to be $t_0 = 1\text{h}56\text{m} \pm 2 \text{ min}$ and the Gaussian half-width, w , was found to be $16 \pm 2 \text{ min}$. This fit is shown in Fig. 8 as the solid curve.

3.3. Double station analysis

Standard procedures for reduction of meteors observed at two stations have been developed by several authors including Wray (1967), Cepelcha (1987) and Hawkes et al. (1993), and will not be repeated here. A detailed explanation of the specific procedures used for these video data can be found in Campbell et al. (2000).

The campaign geometry favoured double-station analysis as camera “pairs” were established at the two main sites, separated by 48.5 km. In the final analysis, two sets of camera pairings produced useable results, cameras F and K and cameras E and J. The camera fields were optimized for overlapping at heights of approximately 160 and 110 km for camera pairs KF and EJ, respectively. The former higher height intersection was specifically chosen to look for faint, high altitude Leonids.

Double-station Leonids were found by comparing times of appearance of meteors at each site. Many false associations were still produced due to the high Leonid rates and a further test was performed by examining the resulting double-station solutions for unphysical trajectory solutions (i.e. with start height $> 250 \text{ km}$ or end heights $< 40 \text{ km}$, etc.). After all double-station associations were properly established, the list was then further reduced by retaining only Leonid meteors — these were found by constraining the resulting single-station great-circle paths for each measured trail to lie within less than 10° of the Leonid radiant. Finally, the double-station solutions were examined to determine if any radiant solutions were more than 10° from the Leonid radiant — these were removed as possibly spurious. This will tend to bias the final radiant determinations, but only a relatively few (less than 5% of the total) were found to be outliers at this level, so it is expected to be a small effect.

After this selection procedure was applied, a total of 114 double station Leonids were found from the EJ camera pair and 118 for the FK pairing over the interval 0.5–3 UT on 18 November 1999. Average quantities for each double-station camera dataset are given in Table 3. Note that for these camera pairings, one camera was a Gen II intensifier (E,F) and

Table 3
Average properties for each Leonid two-station camera pair dataset^a

Camera pairing	EJ (115 Leonids)	FK (118 Leonids)
Average RA (α)	$153.0 \pm 0.1^\circ$	$153.1 \pm 0.1^\circ$
Average DEC (δ)	$21.6 \pm 0.1^\circ$	$21.3 \pm 0.3^\circ$
Average begin height (km)	123.4 ± 1.5	128.1 ± 1.6
Average height of maximum luminosity (km)	108 ± 1.4	118 ± 1.4
Average end height (km)	96.8 ± 1.4	112.8 ± 1.3
Average trail length (km)	29.4 ± 1.3	18.2 ± 0.8
Average mass (kg)	1.6×10^{-6}	4.0×10^{-6}
Average maximum magnitude	1.6 ± 0.1	0.6 ± 0.2
Average range to mid-point of trail (km)	142.2 ± 2.8	135.2 ± 2.3
Average number of frames per meteor	14.0 ± 0.5	9.7 ± 0.4

^aThe radiant positions are referenced to J2000 $\lambda = 235.3^\circ$. Magnitude and mass data refer to the Gen II cameras in each pairing (E,F). Note that the FK pairing is optimized for triangulation at heights of 160 km and that for EJ at 110 km.

one a Gen III (J,K). As the spectral response and sensitivity in general is different for these two types of systems, the absolute values of the masses tend to be different between the cameras for the same event (but with no clear systematic trend). The average values thus given for mean mass refer to cameras E and K (the Gen II’s in each pairing). We have adopted the use of the Gen II masses in all that follows for consistency with previous work and because the Gen II systems tend to have a more visual-like spectral response.

The most unbiased height distribution is found by using the heights determined for the wider of the two cameras in each pair (cf. Campbell et al. (2000) for a more complete discussion). Inclusion of heights from the narrow field of view cause large height biases as most meteors begin or end off-screen. Indeed, for all the double-station Leonid events examined here none which were seen by both the narrow and wide field systems ended outside the fields of view of the wide field cameras.

To compute the true “unbiased” height distribution from that observed, we calculated the fraction of meteors seen at height intervals of 5 km starting at 60 km altitude, using the measured field sizes and pointing directions for each camera pair from the night of 18 November 1999 in a Monte Carlo simulation. In this simulation, a meteor is “detected” if it can be viewed in the fields of both cameras using various ablation heights and an average trail length of 20 km. The resulting geometrical sensitivities as a function of height for the two camera setups is shown in Fig. 9. It can be seen that the geometry for the FK combination results in a much more sharply peaked height sensitivity compared to the EJ pairing, due partly to the narrow field of view of K. This fact is reflected by the larger average heights in Table 3 for FK Leonids and the much smaller dispersion between beginning and ending height in that sample.

As a result, the most unbiased height sample is from camera E. In Fig. 10, we have taken the observed beginning

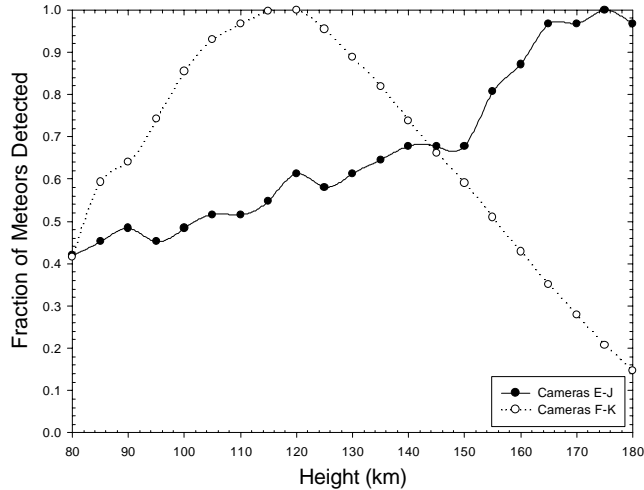


Fig. 9. Relative observational efficiency for meteors ablating at different heights. The detection efficiency is shown for the two camera pairings, cameras EJ (optimized for 110 km height intersection) and camera FK (optimized for 160 km height intersection). The narrower bias curve for the FK pair lower in altitude is due to the much narrower field of view of camera K compared to the wider field EJ pairing, which have a concomitant broader height detection efficiency.

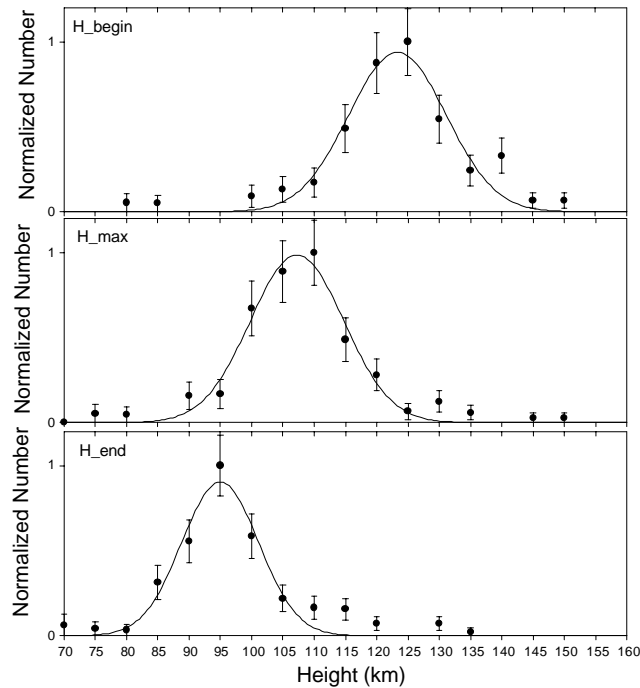


Fig. 10. Corrected relative height distribution for the 1999 Leonids on 18 November 1999 from observations of camera E. Shown are the beginning heights, height at maximum brightness and the end height. The individually measured heights are accurate to ~ 2 km.

heights, heights of maximum brightness and end heights and weighted the distributions by the geometrical bias given in Fig. 9 for the EJ combination. We have not incorporated the physical fading of meteors at greater distances from the camera — for the highest heights of interest where significant numbers of Leonids are present (about 150 km) this

Table 4

Gaussian fit parameters and goodness of fit (correlation coefficient between observed distribution and fit with one equal to a perfect correlation) found for the height distributions of the storm component of the 1999 Leonids from double-station video results for camera E^a

	h_0 (km)	w (km)	Goodness of fit
Beg. height	123.3 ± 0.7	7.81 ± 0.7	0.93
Max. height	107.3 ± 0.42	7.5 ± 0.4	0.97
End height	95.0 ± 0.56	6.2 ± 0.6	0.93

^aAll meteors began and ended in the field of view.

would result in an additional $\sim 20\%$ correction to the numbers as given, which is generally within the statistical error margins.

As can be seen from Fig. 10, the begin, maximum and end heights behave much as expected, shifting to lower altitudes, respectively. We note that the flat light curves characteristic of many Leonids implies that the height of maximum brightness is likely to be in error by several km and hence this is the least precise height measure of the three terms.

The shapes of each height distribution are well approximated by a three-parameter Gaussian fit. This provides a direct measurement of the zone of ablation for the storm component of Leonid meteoroids in the mass range ($\sim 10^{-6}$ kg) accessible to the cameras. The fit is of the form:

$$N = \exp \left[-0.5 \left(\frac{(h - h_0)}{w} \right)^2 \right], \quad (9)$$

where N is the peak-normalized number of Leonids, h is the height (in km), h_0 is the average Gaussian height and w is the width of the distribution in km. Table 4 summarizes the measured fit parameters to each distribution.

We also examined the variation of beginning and end heights as a function of mass/magnitude and found only a very weak trend of lower end heights and higher beginning heights for larger Leonids. This is very similar to the findings for the 1998 Leonids (Campbell et al., 2000).

While some high-altitude (> 140 km) Leonid beginning heights are present in the sample, the relative lack of very high Leonids (> 160 km) (despite the fact that significant biases in the pointing geometries do not begin until ~ 190 km) from both camera pairings is generally consistent with double-station video results found in 1998 (cf. Campbell et al. (2000)) and suggests that the observation of extreme beginning heights (eg. Fujiwara et al., 1998; Spurny et al., 2000) is confined to processes peculiar to larger Leonids. As noted by Campbell et al. (2000), the need to explain these higher video-altitude Leonids still suggests a volatile organic component in small Leonids or that some high-energy process of ablation/atmospheric interaction may be present. We note that our begin heights are some 10 km higher than those found by Betlem et al. (2000) for photographic Leonids, while our end heights are 5 km lower. This is unsurprising given the greater sensitivity of the video systems.

Using the combined results from cameras E and F, we derive the relationship between the maximum magnitude (M), the mass (in kg) and the zenith angle at entry as

$$M = -11.56 (\pm 0.73) - 2.14 (\pm 0.12) \log(m) - 0.04 (\pm 2.40) \log(\cos(z)). \quad (10)$$

This can be compared to the relation:

$$M = -8.76 (\pm 0.46) - 1.89 (\pm 0.07) \log(m) - 1.35 (\pm 0.63) \log(\cos(z)) \quad (11)$$

derived for the 1998 Leonids by Campbell et al. (2000), showing a stronger dependence on mass and weaker dependence on zenith angle than was found in 1998. These relations are derived via a three-parameter regression fit between apparent maximum magnitude, photometric mass and zenith angle. There is also an apparent systematic shift to brighter magnitudes for 1999 Leonids, perhaps the result of somewhat different reduction methods.

As with earlier Leonid video results, we find that the trail length is correlated with the mass and entry angle, with larger Leonids and shallower paths tending to produce longer trail lengths. Fig. 11 shows the combined results for all cameras. To select only the very best data, only Leonids which began and ended entirely within the video field have been included for the Gen II cameras. As a result, the error in the trail length is less than 1 km for any one datum. Additionally, some Leonids may have improper measurements or large measurement errors, so we have imposed a further test whereby the trail length/duration (giving an average velocity) must fall within the range of 55–80 km s⁻¹ to be considered reasonable. The explicit relationship between trail

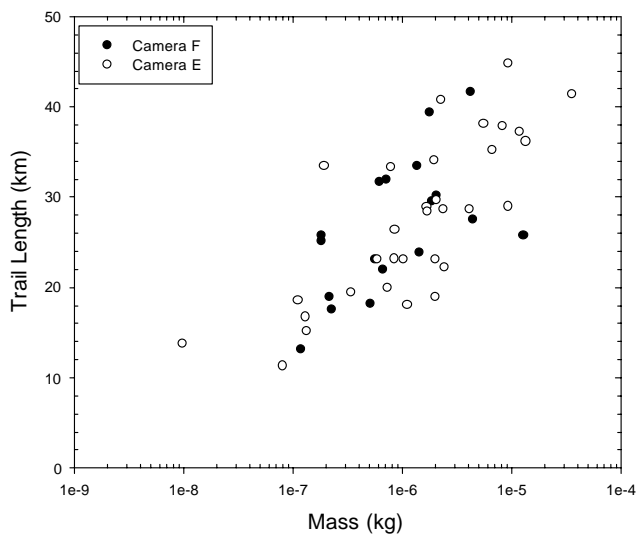


Fig. 11. Observed trail lengths as a function of Leonid mass for all cameras. Note that only Leonids which began and ended completely on the screen have been included. As well, only those Leonids with measured velocities (from trail length/duration) from 55 to 80 km s⁻¹ have been included to remove any improper measurements.

length (dL in km), zenith angle (z) and mass (in kg) for the 1999 Leonids was found via a three-parameter regression amongst these quantities to be:

$$dL = 106.8 (\pm 13.2) - 29.04 (\pm 11.6) \cos(z) + 9.19 (\pm 1.15) \log(m) \quad (12)$$

as compared to

$$dL = 110.5 (\pm 7.1) - 12.5 (\pm 9.3) \cos(z) + 12.8 (\pm 0.90) \log(m) \quad (13)$$

found in the 1998 analysis.

Clearly, the dependence on zenith angle and mass is even greater in 1999 than was found in 1998 but this may be an artifact of the narrower windows (and hence smaller range of radiant elevations) for 1999 data. Also, like the 1998 data only a very weak flattening in the curve at the smallest masses is apparent. This flattening is expected if Leonids consist primarily of small grains of some characteristic size as would be expected for dust-ball meteoroids (cf. Campbell et al., 2000). However, the scatter in 1999 is greater than that found in the 1998 Leonid data, so the effect is even more subtle and largely masked by scatter so no definite conclusions in this regard can be reached.

In addition to heights and trail lengths, the double station results permit determination of radiant positions for individual Leonids. The average radiant position for each camera pairing is shown in Table 3. Within error, the averages for the radiant positions are equal for both camera pairs. Note that all radiant coordinates are referenced to $\lambda = 235.3^\circ$ (J2000). The EJ pairing, however, produced significantly more precise radiant positions than those found from FK, in part because of overall better geometry for the pairing of the former. Our weighted averaged double-station radiant position centred about the Leonid peak is found to be $\alpha = 153.1 \pm 0.1^\circ$ and $\delta = 21.5 \pm 0.2^\circ$. This compares well

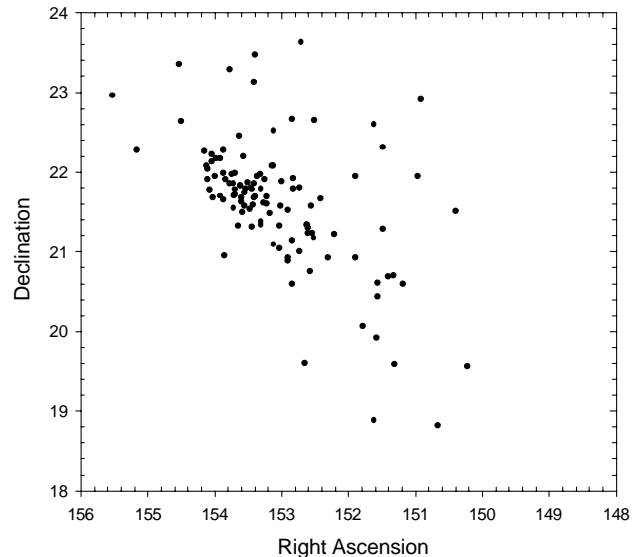


Fig. 12. Double-station radiant positions for camera EJ Leonids.

with the multi-station photographically determined average radiant position of $\alpha = 153.67 \pm 0.05^\circ$ and $\delta = 21.7 \pm 0.05^\circ$ (Betlem et al., 2000) for larger Leonids and $\alpha = 153.6 \pm 0.1^\circ$ and $\delta = 21.9 \pm 0.1^\circ$ found from single-station video results (Rendtel et al., 2000). The scatter for individual radiant determinations is shown in Fig. 12 for the EJ camera pair. A denser clustering between $\alpha = 153\text{--}154^\circ$ and $\delta = 21\text{--}22^\circ$ is evident, but the much tighter clustering noted by Betlem et al. (2000) is not verifiable with these video data as the precision for individual measurements is less than that for photographic results. Typical errors for each datum are of order 0.5° , however some larger values are also present. We believe most of the broader scatter is measurement error and not intrinsic to the radiant at these Leonid masses.

4. Discussion and conclusions

Examination of multi-station LLLTV observations of the 1999 Leonids from Israel has shown that for the video Leonid magnitudes samples, the mass distribution index during the course of the Leonid storm was constant near $s = 1.75$. No variation across the storm profile was clearly detected, though any such variation may be masked by small number statistics. This is similar to the results found visually by Arlt et al. (1999) and Gural and Jenniskens (2000). We find no clear evidence for relative roll-off at low or high masses as reported by Rendtel et al. (2000) and Arlt et al. (1999) in the Leonid population, but caution again that our number statistics are still relatively small.

The video storm flux averaged over all reduced cameras averaged 0.81 ± 0.06 meteoroids $\text{km}^{-2} \text{hr}^{-1}$ $M_v < +6.5$ for 15 min binning and 0.99 ± 0.11 meteoroids $\text{km}^{-2} \text{hr}^{-1}$ $M_v < +6.5$ at 3 min intervals. The smaller temporal resolution reveals a broad plateau in flux lasting from approximately $\lambda_0 = 235.276\text{--}235.285^\circ$ (J2000.0). At least one significant feature in the rate curve is apparent near 235.272° , corresponding to the expected time for encounter with material released in 1932. That both the 1899 and 1932 ejections contributed to the 1999 Leonid storm have previously been suggested by Arlt et al. (1999) on the basis of numerical modelling. A similar feature has been noted by Arlt et al. (1999) and Rendtel et al. (2000) from visual and video observation. The flux profile is found to have a slightly longer rise than fall from maximum. Gaussian fits to the profile show the Gaussian half-width of the dust-trail associated with the Leonid storm in 1999 suggests that the streamlet ejected from 1899/1932 is of order 10^5 km in total thickness perpendicular to the Leonid stream orbital plane.

From de-biased double-station observations, we find that the Leonid height distribution does not have a particularly high altitude tail at the masses investigated ($\sim 10^{-6}$ kg), similar to previous findings (e.g. Campbell et al., 2000). We have found that the relationship between mass, magnitude, entry angle and trail length are somewhat different from what was found for the 1998 Leonids, but the scatter in

the data make it difficult to firmly conclude that this might be due to real physical differences between meteoroids in the different years. The mean radiant position was found to be $\alpha = 153.1 \pm 0.1^\circ$ and $\delta = 21.5 \pm 0.2^\circ$ (J2000), with some hint of a more compact radiant grouping within the range $\alpha = 153\text{--}154^\circ$ and $\delta = 21\text{--}22^\circ$, consistent with the smaller storm meteoroids of younger age having less orbital dispersion than the average Leonid stream meteoroid.

Acknowledgements

Funding for this study was provided by the United States Air Force, the National Reconnaissance Office of the United States, the Canadian Space Agency, the European Space Agency, the Canadian Department of National Defence, the Defence Research Establishment Ottawa, as well as individual grants from the Natural Sciences and Engineering Research Council (NSERC) (R. Hawkes and J. Jones).

The Wise Observatory provided support for the Israel deployment and we thank Noah Brosch for local organization. M. Connors, D. Jewell, S. Nikolova, J. Thorne and S.P. Worden provided assistance with the gathering of observations from Israel. We thank V. Porubčan and an anonymous referee for numerous helpful comments on an earlier version of this work. This is LA-UR-01-1168.

References

- Arlt, R., Rubio, L., Brown, P., Gyssens, M., 1999. Bulletin 15 of the International Leonid watch: first global analysis of the 1999 Leonid storm. WGN JIMO 27 (6), 286–295.
- Betlem et al., H., 2000. (8 co-authors), Precise trajectories and orbits of meteoroids from the 1999 Leonid meteor storm. Earth Moon Planets 82–83, 277–285.
- Brown, P., 1999. The Leonid meteor shower: historical visual observations. Icarus 138, 287–308.
- Brown, P., Arlt, R., 2000. Detailed visual observations and modelling of the 1998 Leonid shower. Mon. Not. R. Astron. Soc. 319, 419–428.
- Brown et al., P., 2000. (and 40 co-authors), Global ground-based electro-optical and radar observations of the 1999 Leonid shower: first results. Earth Moon Planets 82–83, 167–191.
- Campbell, M.D., Hawkes, R.L., Babcock, D., 1998. Leonid light curves and implications for physical structure. Final task report #2, contract report # 5FUSA-7-J151/001/SV.
- Campbell, M.D., Brown, P.G., Leblanc, A.G., Hawkes, R.L., Jones, J., Worden, S.P., Correll, R.R., 2000. Image-intensified video results from the 1998 Leonid shower: I. atmospheric trajectories and physical structure. MAPS 35, 1259–1267.
- Ceplecha, Z., 1987. Geometric, dynamic, orbital and photometric data on meteoroids from photographic fireball networks. Bull. Astr. Inst. Czech. 38, 222–234.
- Fujiwara, V., Ueda, M., Shiba, Y., Sugimoto, M., Kinoshita, M., Shimoda, C., Nakamura, T., 1998. Meteor luminosity at 160 km altitude from TV observations for bright Leonid meteors. Geophys. Res. Lett. 25, 285–288.
- Gural, P., Jenniskens, P., 2000. Leonid storm flux analysis from one Leonid mac video AL50R. Earth Moon Planets 82–83, 221–249.
- Hawkes, R.L., Mason, K.I., Fleming, D.E.B., Stultz, C.T., 1993. Analysis procedures for two station television meteors. In: Ocanás,

- D., Zimnikoval, P. (Eds.), Proceedings of the International Meteor Conference 1992. pp. 28–43.
- Hawkes, R.L., 2002. Detection and analysis procedures for visual, photographic and image intensified CCD meteor observations. In: Murad, E., Williams, I.P. (Eds.), *Monograph on Meteors*. Cambridge University Press, Cambridge, in press.
- Jenniskens, P., Crawford, C., Butow, S.J., Nugent, D., Koop, M., Holman, D., Houston, J., Jobse, K., Kronk, G., Beatty, K., 2000. Lorentz shaped comet dust trail cross section from new hybrid visual and video meteor counting technique — implications for future Leonid storm encounters. *Earth Moon Planets* 82–83, 191–209.
- McNaught, R., Asher, D.J., 1999a. Variation of Leonid maximum times with location of observer. *MAPS* 24, 975–978.
- McNaught, R., Asher, D.J., 1999b. Leonid dust trails and Meteor Storms. *WGN JIMO* 27 (2), 85–102.
- Murray, I., Hawkes, R.L., Jenniskens, P., 1999. Airborne intensified charge-coupled device observations of the 1998 Leonid shower. *MAPS* 34, 949–958.
- Murray, I.S., Beech, M., Taylor, M., Jenniskens, P., Hawkes, R.L., 2000. Comparison of 1998 and 1999 Leonid light curve morphology and meteoroid structure. *Earth Moon Planets* 82–83, 351–367.
- Rendtel, J., Molau, S., Koschny, D., Evans, S., Okamura, O., Nitschke, M., 2000. Video observation of the 1999 Leonid Meteor storm recorded at different locations. *WGN JIMO* 28 (5), 150–165.
- Simek, M., Pecina, P., 2001. Radar observations of the Leonids in 1998 and 1999. *Astron. Astrophys.* 365, 622–626.
- Singer, W., Molau, S., Rendtel, J., Asher, D.J., Nitchell, N.J., von Zahn, W., 2000. The 1999 Leonid meteor storm: verification of rapid activity variations by observations at three sites. *Mon. Not. R. Astron. Soc.* 318, L25–L29.
- Spurny, P., Betlem, H., van't Leven, J., Jenniskens, P., 2000. Atmospheric behaviour and extreme beginning heights of the 13 brightest photographic Leonids from the ground-based expedition to China. *MAPS* 35, 243–249.
- Wray, J.D., 1967. *The Computation of Orbits of Doubly Photographed Meteors*. University of New Mexico Press, Albuquerque, USA.
- Verniani, F., 1965. On the luminous efficiency of meteors. *Smithson. Contr. Astrophys.* 9, 141–172.
- Yeomans, D.K., Yau, K.K., Weissman, P.R., 1996. The impending appearance of comet Tempel–Tuttle and the Leonid meteors. *Icarus* 124, 407–413.